Molecular Catalysis 565 (2024) 114386

Contents lists available at ScienceDirect

Molecular Catalysis

journal homepage: www.journals.elsevier.com/molecular-catalysis

# Computational screening of metalloporphyrin catalysts for the activation of carbon dioxide

Amira Tasnima Uddin [a], Qi Zhao [a], Dimitrios Toroz [a], Rachel Crespo-Otero [b,*], Devis Di Tommaso [a,c,*]

[a] Department of Chemistry, School of Physical and Chemical Sciences, Queen Mary University of London, Mile End Road, London, E1 4NS, UK
[b] Department of Chemistry, University College London, 20 Gordon St, London, WC1H 0AJ, UK
[c] Digital Environment Research Institute, Queen Mary University of London, Empire House, 67-75 New Road, London E1 1HH, UK

ARTICLE INFO

*Keywords:*
Electrochemical $CO_2$ reduction
Metalloporphyrin
$CO_2$ activation
Density functional theory

ABSTRACT

Electrocatalytic $CO_2$ reduction ($eCO_2R$) to value-added chemicals offers a promising route for carbon capture and utilization. Metalloporphyrin (M-POR) is a class of catalysts for $eCO_2R$ that has drawn attention due to its tuneable electronic and structural properties. This work presents a computational screening, based on density functional theory calculations, of one of the key steps in the $eCO_2R$: the adsorption of $CO_2$ on 110 M-PORs with varying peripheral ligands, metal centres, and oxidation states, to understand how these factors can influence $CO_2$ activation. A set of criteria was used to shortlist M-PORs based on their ability to lengthen the C–O bond, bend the O–C–O angle, bind $CO_2$, and donate charge from the metal of the M-POR to the carbon of $CO_2$. 16 systems were selected for their potential to activate $CO_2$. These systems predominantly have the electron configuration of the metal centre in the d[6] and d[7] configurations. Natural bond orbital analysis revealed the impact of electron-withdrawing groups in the system, which increases orbital splitting and, consequently, lowers the ability of the M-POR to activate $CO_2$. Second-order perturbation theory analysis confirms that the presence of electron-donating groups in the ligand structure enhances $CO_2$ activation. This work demonstrates the interconnected effect of peripheral ligands, metal centres, and oxidation states in M-PORs on their ability to adsorb and activate $CO_2$, thereby establishing structure-activity relationships within M-PORs.

## 1. Introduction

The extensive use of fossil fuels has led to an increase in atmospheric carbon dioxide ($CO_2$), a key greenhouse gas responsible for absorbing and radiating heat, thereby destabilizing Earth's ecosystem [1]. This, along with limited energy sources, poses a serious global challenge [2,3]. Carbon capture and utilization (CCU) techniques are important for bridging the gap between our high-carbon industries and a sustainable, low-carbon future. CCU allows $CO_2$ to be used as a valuable resource rather than accumulating in the atmosphere, thereby enabling a circular economy [4]. The thermo-catalytic transformation of $CO_2$ produces one-carbon ($C_1$) molecules such as carbon monoxide (CO), methane ($CH_4$), or methanol ($CH_3OH$) in high yields, but it requires high temperatures (around 573 K) and is therefore energy-intensive [5].

Electrochemical $CO_2$ reduction ($eCO_2R$) is a promising CCU technique that offers a pathway to produce not only $C_1$ molecules but also multi-carbon ($C_{2+}$) products such as ethylene ($C_2H_2$), ethanol ($C_2H_5OH$), and 2-propanol ($(CH_3)_2CHOH$) [6–9]. By using renewable electricity, the $eCO_2R$ can generate "electrofuels", a term used to describe renewable electricity being stored in chemical bonds [10]. This allows for high-energy-density storage from wind or solar generators to serve as a highly flexible renewable source of traditionally fossil-derived resources [11].

The challenge in $eCO_2R$ lies in the high overpotential required to remove the first electron from $CO_2$ and form the $CO_2$ radical [12]. It is commonly assumed that the reaction is difficult because $CO_2$ is an inert molecule [13,14]. However, it was recently reported that the electrocatalytic environment also stabilises the $CO_2$ radical, further limiting the kinetics of the process [15,16]. Therefore, a good electrocatalyst would lower the overpotential and make it more feasible to remove the first electron from $CO_2$. Moreover, the product of $eCO_2R$ is usually a mixture of gaseous and liquid products [17,18], which makes the selectivity of this reaction a further technical challenge, thereby limiting the ability to scale up $eCO_2R$ for practical, commercial applications [19].

* Corresponding authors.
*E-mail addresses:* r.crespo-otero@ucl.ac.uk (R. Crespo-Otero), d.ditommaso@qmul.ac.uk (D. Di Tommaso).

https://doi.org/10.1016/j.mcat.2024.114386
Received 30 April 2024; Received in revised form 19 June 2024; Accepted 9 July 2024
Available online 17 July 2024

The activation and selectivity of the $eCO_2R$ can be altered by a complex interplay of four factors: solution identity (the nature and concentration of the electrolyte solution); mass transport (the rate at which $CO_2$ and other reactants are transported to the catalyst surface); surface structure (the size, shape, and composition of the catalyst surface); catalytic properties (the ability of the catalyst to activate $CO_2$ and promote its reduction to desired products) [10]. In particular, the choice of a catalytic system whose electronic and structural properties can be finely tuned to improve the activation of $CO_2$ is crucial for the design of efficient electrocatalytic devices [20].

Among the most promising $eCO_2R$ catalysts, metalloporphyrin (M-POR) has attracted significant interest [20]. M-POR is a molecular catalyst consisting of a central metal atom surrounded by a cyclic carbon-nitrogen ring composed of four modified pyrrole subunits. The molecular structural framework of M-PORs offers a unique combination of tunability of the peripheral ligands, the flexibility of the metal centre, and versatility of the oxidation states, which can be exploited to tailor the catalytic properties of M-PORs for $eCO_2R$ [21] and other electrocatalytic reactions [22]. For example, Sen et al. reported that the kinetics of the $eCO_2R$ to CO by iron porphyrin complexes can be tuned by changing the second sphere hydrogen bonding residues, without significantly modifying the first coordination sphere functionalities [23]. It was shown that pre-organising a hydrogen bonding network at the distal site can adjust the rate of $CO_2$ production by up to 1000 times. This enhanced selectivity in $eCO_2R$ provides valuable insights into catalytic processes. Additionally, Lv et al. recently demonstrated the use of a hierarchical M-POR framework to achieve highly selective and efficient $eCO_2R$ to CO [22]. The synthesis of M-PORs using Earth-abundant elements such as iron [24,25] or nickel [26] reduces the synthetic cost of M-PORs compared to catalysts made from precious and rare metals such as gold [27], silver [28], rhodium [29], iridium, [30] and palladium [31]. These catalysts are expensive, so lower-cost and more sustainable alternatives are needed to develop a long-term ecologically and economically sustainable process.

In a M-POR, the metal centre can also adopt either a neutral, $[M\text{-}POR]^0$, single reduced, $[M\text{-}POR]^-$, or doubly reduced, $[M\text{-}POR]^{2-}$, oxidation state [32]. This can be beneficial for addressing the competition with the hydrogen evolution reaction (HER, $H^+ + e^- \rightarrow \frac{1}{2} H_2$). For example, a computational study based on density functional theory (DFT) by Masood et al. revealed that weakening the nucleophilicity of the metal centre promotes $CO_2$ binding compared to proton binding. This enhances the selectivity towards the $eCO_2R$ [33], as the initial binding of either proton or $CO_2$ dictates the reaction route. Thus, $CO_2$ binding is crucial. In this study, it was found that $[Fe\text{-}POR]^-$ and $[Co\text{-}POR]^-$ have low electron density on their metal centres, and therefore, are less nucleophilic. This does not enhance reactivity towards protons, and the catalyst is open to $CO_2$ adsorption, leading to CO formation. On the other hand, catalysts like $[RhP]^0$ and $[IrP]^0$ possess metal centres with high electron density, making them highly nucleophilic, which favours proton binding over $CO_2$, leading to preferential hydrogen evolution. Another DFT investigation also showed the significant influence of the initial oxidation state of the metal centre on the reaction energetics [34]. This study examined Fe, Co, and Ni and reported that the neutral $[M\text{-}POR]^0$ exhibited poor $CO_2$-to-formate conversion due to weak $*COO^-$ binding. In contrast, $[M\text{-}POR]^{-1}$ and, even more favourably, $[M\text{-}POR]^{-2}$ exhibited higher Faraday efficiencies for CO formation. A DFT investigation by Corbin et al. further highlighted the significant influence of the metal centre oxidation state on the reaction energetics [35]. Their study focused on Fe, Co, and Ni, and found that $[M\text{-}POR]^{-2}$ was the most favourable for achieving higher selectivity towards the $eCO_2R$ to CO. From a computational standpoint, focusing on a single metal atom catalyst, such as M-POR, is also a valuable approach for understanding the activation of $CO_2$, because it allows for a simplified analysis of the system, making it easier to identify the key factors that control the $eCO_2R$ [35–38].

A key step in the $eCO_2R$ is the adsorption and activation of $CO_2$. Before its dissociation, $CO_2$ can exist in a bent state (activated state) on the catalyst surface [39]. This is the result of charge transferred from the catalyst to the $CO_2$ molecule, which in turn results in the elongation of the C–O bonds and a decrease in the O–C–O bond angle (linear to bent mode) [40]. As previous computational studies of the $CO_2$ activation on M-POR have covered a limited number of catalysts, in this study extensive DFT calculations were performed to find key properties of M-POR that enhance $CO_2$ activation. For this purpose, the computational database of catalysts in Fig. 1 were generated based on well-known M-PORs built by varying the metal (M), substituents (POR), and oxidation states of the metal (+2, +1, 0) [36]. For $[M\text{-}POR_{1\text{–}9}]$ in Fig. 1, the systems explored contained the metals Ni, Fe, Cu and Co with the overall M-POR charge being neutral, singly, and doubly reduced. The $[M\text{-}POR_{10}]$ and $[M\text{-}POR_{11}]$ with only Ni metal centre were considered in the doubly reduced state as they could potentially be included in future work on carbon frameworks due to their carbonaceous ligands. This gives a total of 110 M-POR systems. The objective is to identify which structural and electronic factors in M-POR enables $CO_2$ activation, as measured by specific indicators: C–O elongation, O–C–O bending, charge transfer, and first and second electron affinities [35,38,41].

## 2. Computational details

The NWChem code (version 6.6) [41] was used to conduct the full geometry optimizations of the M-PORs in Fig. 1, while Gaussian [42] was used to evaluate the solvation energy contribution and conduct electronic structure analysis. All calculations were conducted at the DFT level of theory. An extensive benchmark of the exchange-correlation functionals and basis sets was conducted by considering Generalized Gradient Approximation (GGA) (BLYP and PBE) and hybrid GGA functionals (B3LYP and PBE0) together with double-zeta (3-21G, 6-31G(d, p), LANL2DZ) and triple-zeta (SVPD, TZVP) basis sets. As part of the benchmarking, the MP2/TZVP level of theory was also used. The results of this full benchmarking analysis are reported in **Table S1** of Supporting Information, from which it was concluded the B3LYP/LANL2DZ provides the best compromise between accuracy and computational cost. Solvent effects were incorporated with the implicit solvation model Conductor-like Screening Model (COSMO) [43], using water as the solvent, to describe the aqueous environment [44]. The Gaussian code with the B3LYP/LANL2DZ level of theory was used for Hirschfeld charge analysis and Natural Bond Order (NBO) analysis. The binding energy ($E_b$) was calculated using the following equation:

$$E_b = E_{MPOR-CO2} - E_{MPOR} - E_{CO2} \quad (1)$$

where $E_{MPOR-CO2}$ is the optimised energy of the M-POR with $CO_2$ adsorbed, $E_{MPOR}$ is the optimised energy of M-POR, and $E_{CO2}$ is the optimised energy of pristine $CO_2$. The AIM-UC program was then used to produce the Laplacian electron density maps [45]. Electron localisation maps were generated with the Vienna Ab initio Simulation Package (VASP) (version 6.4.0) [41,42], which implements the DFT projector-augmented wave (PAW) [43] approach to describe the electron-ion interaction. The plane-wave energy cut-off was set at 500 eV and the total energy convergence criterion was set to $10^{-6}$ eV. With VASP, the exchange-correlation function was described using the Perdew-Burke-Ernzerhof (PBE)[44] generalized gradient approximation together with Grimme's DFT-D3 [45] correction to describe the nonlocal dispersive interactions. The Γ-point was used to sample the Brillouin zone. The size of the cubic cell was set to 16 Å. For the optimized structures of M-POR and $[M\text{-}POR\cdots CO_2]$ of the metalloporphyrin catalysts that showed activation of $CO_2$, frequency calculations were also conducted to verify they were a minimum on their potential energy surface (all positive frequencies). The analysis of the C—O vibrations $CO_2$ was also used to analyse the activation of the $CO_2$ molecule as a decrease of the stretching mode of adsorbed $CO_2$ compared to the value

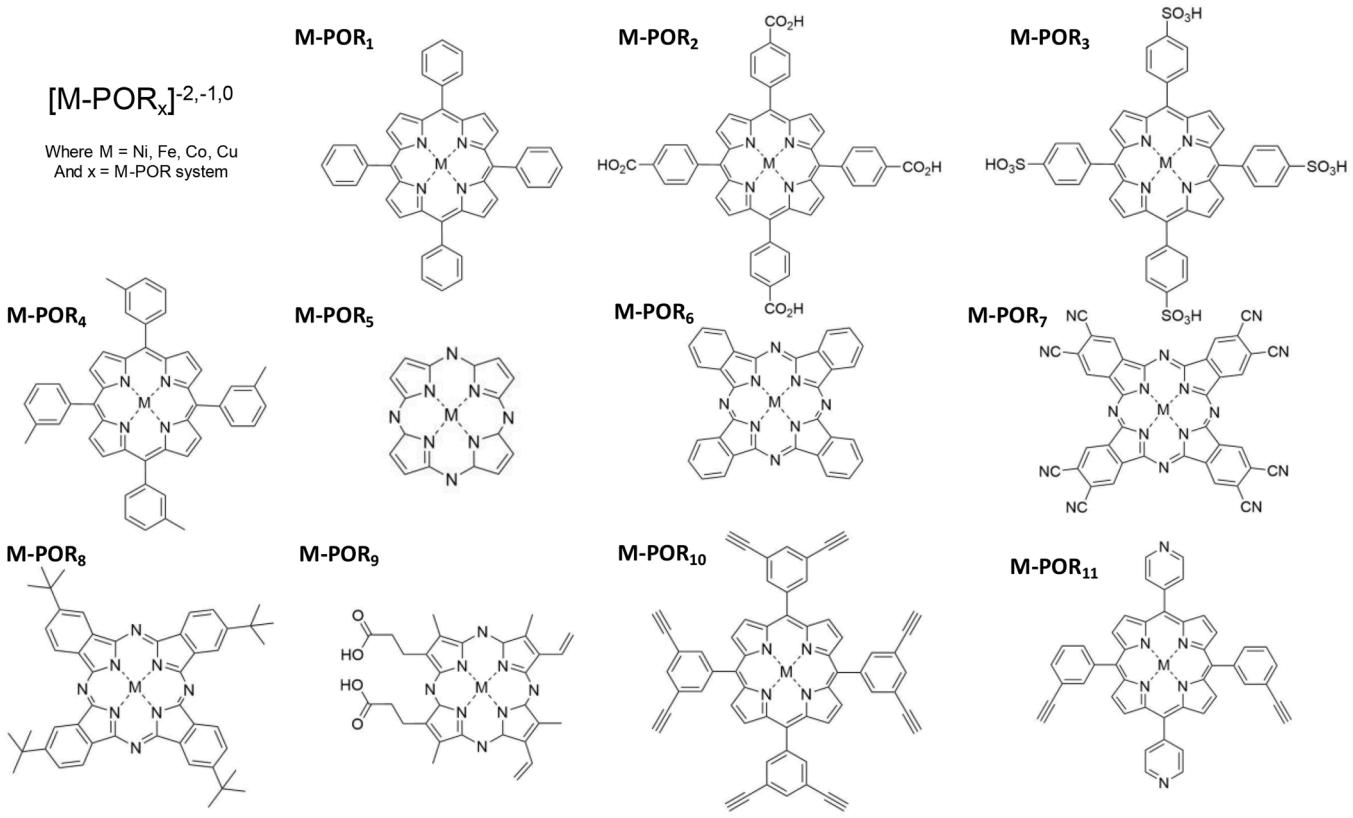


**Fig. 1.** The computational database of 110 metalloporphyrins (M-PORs) with varying metal (M), porphyrin (POR), and oxidation states of the metal (+2, +1, 0). The database was created to investigate the effect of these factors on the catalytic properties of M-PORs for the adsorption and activation of $CO_2$.

of 2285 $cm^{-1}$ in the isolated gas phase molecule correspond to a weakening of the bond. The multiplicity of M-POR was chosen as the one providing the lowest energy of the system. Calculations of [Co-POR$_{3,4,6}$]$^0$, with and without $CO_2$ adsorbed, were also conducted to the effect of multiplicity on $CO_2$ activation (see **Table S6** of Supporting Information). It was found that the multiplicity did not significantly affect the $CO_2$ activation.

## 3. Results and discussion

### 3.1. Adsorption and activation of $CO_2$ on metalloporphyrin

In the gas phase, the $CO_2$ molecule has a linear geometry with a bond angle of 180° and bond lengths of 1.176 Å [40]. Activation of the inert $CO_2$ molecule for chemical reactions involves reducing orbital overlap, achievable through molecular bending or stretching. Specifically, the bending of the $CO_2$ molecule significantly weakens orbital overlap compared to bond elongation [46]. Geometry optimization of $CO_2$ adsorbed on the 110 M-PORs in Fig. 1 was conducted at the B3LYP/LANL2DZ level of theory in order to characterize the activation of $CO_2$ using the following indicators shown in Fig. 2: binding energy ($E_{bind}$); $CO_2$ bending (Δθ); $CO_2$ bond length variation (Δl); Hirschfeld charge transfer (ΔQ). The complete list of computed values for these indicators can be found in **Table S2** of the Supporting Information.

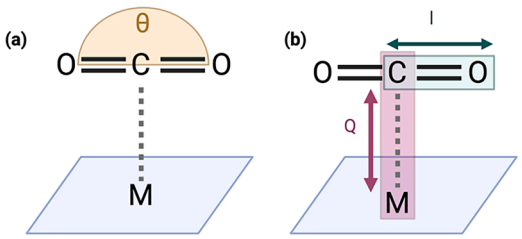


**Fig. 2.** Diagram showing **(a)** the bond angle variation, **(b)** bond length elongation, and charge transferred from the metal (M) of the metalloporphyrin to the $CO_2$ molecule.

While previous computational investigations identified clear correlations between these $CO_2$ activation indicators [47], those studies only compared a limited number of catalyst systems. Instead, a clear correlation between $E_{bind}$, Δl, Δθ, and ΔQ for the $CO_2$ adsorption on the 110 M-POR catalysts was difficult to establish. However, the strongest correlation was found in Fig. 3 between Δθ, Δl, and ΔQ. Typically, when adsorbed to the catalyst site, $CO_2$ can be categorized as either physisorbed (where $CO_2$ retains its structure) or chemisorbed (where $CO_2$ loses its linearity and/or extends its C–O bonds). Thus, the ability of a catalyst to lead to an energetically favourable chemisorbed state has been used in this study as a proxy for catalytic activity towards e$CO_2$R [39,48]. However, the correlation graphs in Fig. 3 **(a-c)** feature a more complex classification with four possible $CO_2$ adsorption categories: (i) fully physisorbed (**F-P**, yellow), characterized by no significant variation of Δθ, Δl, and ΔQ; (ii) fully chemisorbed (**F-C**, orange), exhibiting correlation between the variables, with charge donation showing the most prominent changes; two states characterized by (iii) pronounced bond angle variation and pronounced charge donation but moderate bond elongation (**C-1**, pink), and (iv) 30–40 % variation in bond length, bond angle, and around 20 % in charge donation (**C-2**, blue). Categories **C-1** and **C-2** can be considered intermediary states between full chemisorption and full physisorption, with **C-1** exhibiting a greater propensity for chemisorption while **C-2** leans towards physisorption-like behaviour. A more detailed classification of the types of bonding can be seen in Table 1, where each relationship presented in Fig. 3 has the boundaries for the variation of the bond length, Δl(C—O), bond angle, Δθ(C—O), and charge transfer to the C atom ΔQ(C) used to define the **F-C, F-P, C-1**, and **C-2** categories. If the structure of the $CO_2$···M-POR complexes did

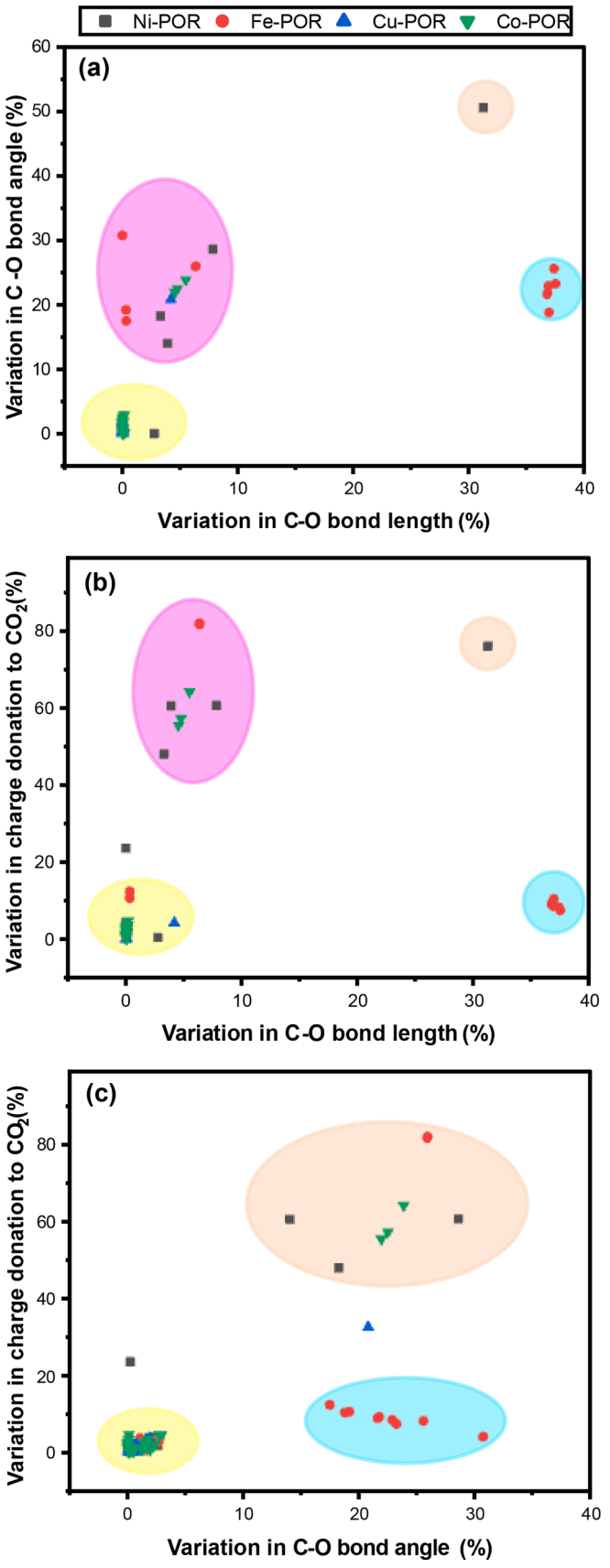


*(caption on next column)*

**Fig. 3.** The relationships between the variation in C—O bond length and the $CO_2$ bond angle, as well as the charge donation from M-POR to $CO_2$, are depicted. The color codes represent different levels of chemisorption: **F-P** (fully physisorbed, yellow), **C-1** (partial chemisorption, pink), **C-2** (strong chemisorption, blue), and **F-C** (fully chemisorbed, orange). These results were obtained for the M-POR catalysts in all oxidation state. (For interpretation of the references to color in this figure legend, the reader is referred to the web version of this article.)

not fit in **F-C, F-P, C-1**, and **C-2**, it was then classed as non-bonded $CO_2$. This suggests a continuum for the $CO_2$ adsorption behaviour on the M-PORs.

Each graph in Fig. 3 has a different number of systems in each classification, with the number of systems classified in each category listed in Table 2. Most exhibit a fully physisorbed state in all three graphs, but there are some variations. For instance, $[Co\text{-}POR_2]^{-1}$ is considered **F-C** in **(a)** and **(b)**, but **C-2** in **(c)**. Similarly, $[Fe\text{-}POR_6]^0$ and $[Fe\text{-}POR_7]^0$ are **FC** in **(a)**, but **FP** in **(b)** and **C2** in **(c)**. This finding highlights the limitations of using only two descriptors to definitively classify $CO_2$ adsorption as chemisorption or physisorption. The choice of descriptors can significantly influence this categorization, potentially leading to erroneous conclusions about $CO_2$ activation. Therefore, a comprehensive assessment using multiple and relevant descriptors is crucial for accurately distinguishing between chemisorption and physisorption states.

The energetics of the $CO_2$ adsorption process were also calculated to identify any energy barriers hindering the activation of the thermodynamically stable $CO_2$ molecule [46]. In Fig. 4 **(a)**, $[Fe\text{-}POR_8]^{-2}$ was considered for the **F-C** segment. In Fig. 4**(b)**, $[Fe\text{-}POR_4]^{-2}$ and $[Fe\text{-}POR_3]^0$ were considered for the **C1** and **C2** categories, respectively. In Fig. 4**(c)**, the system $[Ni\text{-}POR_2]^{-1}$ was considered for **F-P**. The structures of the respective chemisorbed and physisorbed structures were used as input configurations to compute the energetics in Fig. 4 **(a-c)**. For these systems, constrained optimization with respect to the metal of M-POR and the carbon atom of $CO_2$ was applied to locate any transition states between the physisorbed and chemisorbed states.

The $[Fe\text{-}POR_8]^{-2}$ system in Fig. 4**(a)**, which belongs to the **F-C** segment, shows a global minimum at ~2.5 Å and a local minimum at ~3.5 Å. For this system, $CO_2$ chemisorbs spontaneously onto $[Fe\text{-}POR_8]^{-2}$. Systems $[Fe\text{-}POR_4]^{-2}$ (**C-1**) and $[Fe\text{-}POR_3]^0$ (**C-2**) transitions from a chemisorbed to a physisorbed state can be seen as very similar in Fig. 4**(b)**. For $[Ni\text{-}POR_2]^{-1}$ in Fig. 4**(c)**, a single minimum is observed at 3.5 Å, indicating that this system does not activate $CO_2$. In all M-POR it was seen that $CO_2$ can coordinate through oxygen or carbon.

### 3.2. Electronic structure analysis

To rationalize the differences in adsorption behaviours of the four M-POR···$CO_2$ systems in Fig. 4 **(a-c)**, the electron localization function (ELF) was computed. The ELF quantifies the likelihood of finding an electron in a specific region, providing insights into electron sharing and bonding. The ELF maps in Fig. 5 show the electron clouds around the atoms in each system, where red and orange regions represent high electron density (localization), indicating areas of strong bonding and potential reactivity.

Analysis of the ELF plot in Fig. 5 **(a)** reveals a close interaction between the Ni centre in $[Ni\text{-}POR_2]^{-1}$ and the C atom of $CO_2$. This interaction is evidenced by the high electron density observed between the C and Ni atoms, suggesting strong electron sharing and potential bond formation. The d[9] electronic configuration of Ni in $[Ni\text{-}POR_2]^{-1}$ indicates a half-occupied d orbital (likely $d_{x2\text{-}y2}$) that could potentially donate an electron from $CO_2$ during the interaction. Furthermore, the high electron density around the carbon and subsidiary ligands, particularly the porphyrin, indicates its role in the bending and stretching of the $CO_2$ molecule. This observation suggests that the porphyrin ring actively participates in the interaction with $CO_2$,

**Table 1**
Boundaries used to classify the $CO_2$ adsorption into fully physisorbed (F-P), fully chemisorbed (F-C), and intermediate states between chemisorbed and physisorbed (C-1 and C-2) based on the variation of the bond length, Δl(C—O), bond angle, Δθ(C—O), and charge transfer to the C atom of $CO_2$ ΔQ(C).

| | Fig. 3**(a)** | | Fig. 3(b) | | Fig. 3(c) | |
|---|---|---|---|---|---|---|
| Bonding type | Δl(C—O)% | Δθ(C—O)% | Δl(C—O)% | ΔQ(C)% | ΔQ(C)% | Δθ(C—O)% |
| **F-C** | 0–10 | 10–40 | 0–10 | 40–80 | n/a | n/a |
| **F-P** | 0–5 | 0–5 | 0–10 | 0–20 | 0–5 | 0–5 |
| **C-1** | 25–35 | 45–60 | 25–35 | 60–80 | 40–85 | 10–30 |
| **C-2** | 30–40 | 10–30 | 30–40 | 0–20 | 0–20 | 15–35 |
| **Non-bonded** | >40 | >60 | >40 | >80 | >85 | >35 |

**Table 2**
Number of systems classified in each $CO_2$ adsorption category in Fig. 3 **(a-c)**: **F-C** = fully chemisorbed systems; **F-P** = fully physisorbed; **C-1** = strong chemisorption; **C-2** = slight chemisorption; **N-B** = non-bonded.

| Structures in Fig. 3**(a)** | | | | | |
|---|---|---|---|---|---|
| M-POR | F-C | F-P | C-1 | C-2 | N-B |
| Ni-POR | 2 | 26 | 1 | 0 | 0 |
| Fe-POR | 5 | 16 | 0 | 6 | 0 |
| Cu-POR | 1 | 26 | 0 | 0 | 0 |
| Co-POR | 3 | 24 | 0 | 0 | 0 |
| **Total** | **11** | **92** | **1** | **6** | **0** |
| **Structures in Fig. 3(b)** | | | | | |
| **M-POR** | **F-C** | **F-P** | **C-1** | **C-2** | **N-B** |
| Ni-POR | 2 | 25 | 1 | 0 | 1 |
| Fe-POR | 2 | 19 | 0 | 6 | 0 |
| Cu-POR | 0 | 26 | 0 | 0 | 1 |
| Co-POR | 3 | 24 | 0 | 0 | 0 |
| **Total** | **7** | **94** | **1** | **6** | **2** |
| **Structures in Fig. 3(c)** | | | | | |
| **M-POR** | **F-C** | **F-P** | **C-1** | **C-2** | **Non-bonded** |
| Ni-POR | 0 | 25 | 2 | 0 | 2 |
| Fe-POR | 0 | 16 | 2 | 9 | 0 |
| Cu-POR | 0 | 26 | 0 | 0 | 1 |
| Co-POR | 0 | 24 | 3 | 0 | 0 |
| **Total** | **0** | **91** | **7** | **9** | **3** |

potentially influencing its activation.

In Fig. 5 **(b)**, the ELF for system $[Fe\text{-}POR_4]^{-2}$ indicates the interaction with $CO_2$ to be weaker compared to $[Ni\text{-}POR_2]^{-1}$. While the $CO_2$ molecule remains bent, the stretching is less pronounced, with the electron density primarily concentrated on the O atoms. This suggests a weaker interaction between the Fe centre and $CO_2$ compared to Ni.

Moving to Fig. 5 **(c)**, $CO_2$ coordinated to $[Fe\text{-}POR_3]^0$ exhibits small bending. Notably, the electron density surrounding the $CO_2$ is lower compared to the previous systems, with considerable density observed on the peripheral ligands. This suggests a physisorption process, where weaker long-range interactions dominate over strong chemical bonding with the Fe centre.

Finally, the ELF for $[Fe\text{-}POR_8]^{-2}$ in Fig. 5 **(d)** presents a more complex picture. While high electron density is observed on the peripheral ligands, similar to $[Fe\text{-}POR_3]^0$, it also appears concentrated on the oxygen atoms of $CO_2$. This suggests a potential competition between the binding of O and C to the Fe centre. Interestingly, other systems in the **F-C** series exhibit C binding, implying that additional factors beyond electron density might influence the binding preference such as steric effects or surface area of the M-POR.

The activation of $CO_2$ is a result of the electronic charge transfer from the HOMO of the cluster to the LUMO of the $CO_2$ molecule [49]. To investigate the direction of charge migration between the M-POR and $CO_2$, the energies of the HOMO and LUMO of $Ni\text{-}POR_2]^{-1}$, $[Fe\text{-}POR_4]^{-2}$, $[Fe\text{-}POR_3]^0$, and $[Fe\text{-}POR_8]^{-2}$ has been compared with those of gas-phase $CO_2$ (as shown in Fig. 6). For all systems considered, the energy difference between the HOMO of $CO_2$ and the LUMO of the M-POR (highlighted by grey dashed arrow) is larger than the energy difference of the HOMO of the M-POR and the LUMO of $CO_2$ (purple dashed arrow). For example, the energy difference between the HOMO of $CO_2$ and LUMO of $[Ni\text{-}POR_2]^{-1}$ is 7.59 eV while the energy difference between the HOMO of $[Ni\text{-}POR_2]^{-1}$ and the LUMO of $CO_2$ is 3.25 eV. $[Fe\text{-}POR_4]^{-2}$ shows similar values where the energy difference between the HOMO of $CO_2$ and LUMO of $[Fe\text{-}POR_4]^{-2}$ is 8.51 eV while the energy difference between the $HOMO_{M\text{-}POR}$-$LUMO_{CO2}$ is 3.01 eV.

Consequently, $[Fe\text{-}POR_3]^0$ is the least likely of the four systems to promote the charge transfer from the metal centre to the C of $CO_2$, as it has the largest $HOMO_{M\text{-}POR} - LUMO_{CO2}$ gap (5.57 eV). $[Fe\text{-}POR_8]^{-2}$ has a $HOMO_{M\text{-}POR}$-$LUMO_{CO2}$ gap of 3.67 eV and a $HOMO_{CO2}$-$LUMO_{M\text{-}POR}$ gap of 8.06 eV. Therefore, the charge transfer from the M-POR to the $CO_2$ molecule is more favourable when this occurs in conjunction with the bending of the $CO_2$ molecule, as depicted in Fig. 5**(a)** and **(b)**. The correlation between the $HOMO_{CO2}$-$LUMO_{M\text{-}POR}$ gap and the charge transfer to the C of $CO_2$ (Fig. 3**(c)**) is not necessarily a linear relationship when considering all systems. There is increased charge transfer with decreasing $HOMO_{CO2}$-$LUMO_{M\text{-}POR}$ gap for the systems $[Fe\text{-}POR_3]^0$, $[Ni\text{-}POR_2]^{-1}$, and $[Fe\text{-}POR_4]^{-2}$ (ΔQ(C) of 9.2 %, 60.6 %, and 80.2 % respectively). However, $[Fe\text{-}POR_8]^{-2}$ does not fit this trend as it has a $HOMO_{M\text{-}POR}$-$LUMO_{CO2}$ gap of 3.67 eV and a ΔQ(C) of 4.0 %.

### 3.3. The criteria defining the M-PORs activating $CO_2$

The interaction of $CO_2$ with the 110 M-PORs was further analysed to establish the level of $CO_2$ activation against the following criteria (Table 3):

**Criterion 1** is the strength of $CO_2$ binding with M-POR: the binding energy (ΔE) must be negative but not too large ($\Delta E > -40$ kcal $mol^{-1}$) to avoid catalyst poisoning, i.e., impede further reaction steps [50]. An instance of $CO_2$ poisoning on the M-POR problem arose when researchers utilized isomers of a tetraazamacrocyclic Ni(II) complex in solutions saturated with argon, CO, and $CO_2$ [51–53].

**Criterion 2** is the elongation of the C–O bond: the catalyst must have significant $CO_2$ bond elongation (>15 %) as a computational investigation of $CO_2$ adsorption on metal oxides based on the data mining subgroup-discovery model concluded C–O bond elongation to be the best indicator of $CO_2$ activation [54].

**Criterion 3** is the bending of $CO_2$: the catalyst must also induce a significant Δθ (>15 %) as $CO_2$ bending corresponds to breakage of the sp C hybridisation.

**Criterion 4** is the charge transfer from the metal to $CO_2$: there should be significant Hirschfeld charge variation (>15 %) on the C atom as this reaction is a reduction process.

The following catalysts meet at least two criteria, with one or more possibly meeting an additional criterion: $[Ni\text{-}POR_1]^{-1}$, $[Ni\text{-}POR_3]^{-1}$, $[Fe\text{-}POR_1]^0$, $[Fe\text{-}POR_1]^{-2}$, $[Fe\text{-}POR_2]^0$, $[Fe\text{-}POR_3]^0$, $[Fe\text{-}POR_4]^0$, $[Fe\text{-}POR_4]^{-2}$, $[Fe\text{-}POR_5]^0$, $[Fe\text{-}POR_8]^0$, $[Cu\text{-}POR_5]^{-2}$, $[Co\text{-}POR_2]^{-2}$, $[Co\text{-}POR_4]^{-1}$, $[Co\text{-}POR_5]^{-1}$ (highlighted in green in Table 3). Both Ni-POR catalysts possess a d[9] electronic configuration for the Ni atom. Among the neutral iron (d[6]) based catalysts, $[Fe\text{-}POR_2]^0$, $[Fe\text{-}POR_3]^0$, and $[Fe\text{-}POR_4]^0$ exhibit the highest $CO_2$ activation effectiveness. $[Fe\text{-}POR]^{-2}$ and $[Co\text{-}POR_{2,4,5}]^{-1}$ have a d[8] configuration, which is also moderately effective for $CO_2$ activation. However, $[Co\text{-}POR_{2,4,5}]^{-1}$ demonstrates the lowest reactivity among the shortlisted catalysts. As expected, [Cu-POR] catalysts show poor $CO_2$ activation due to their

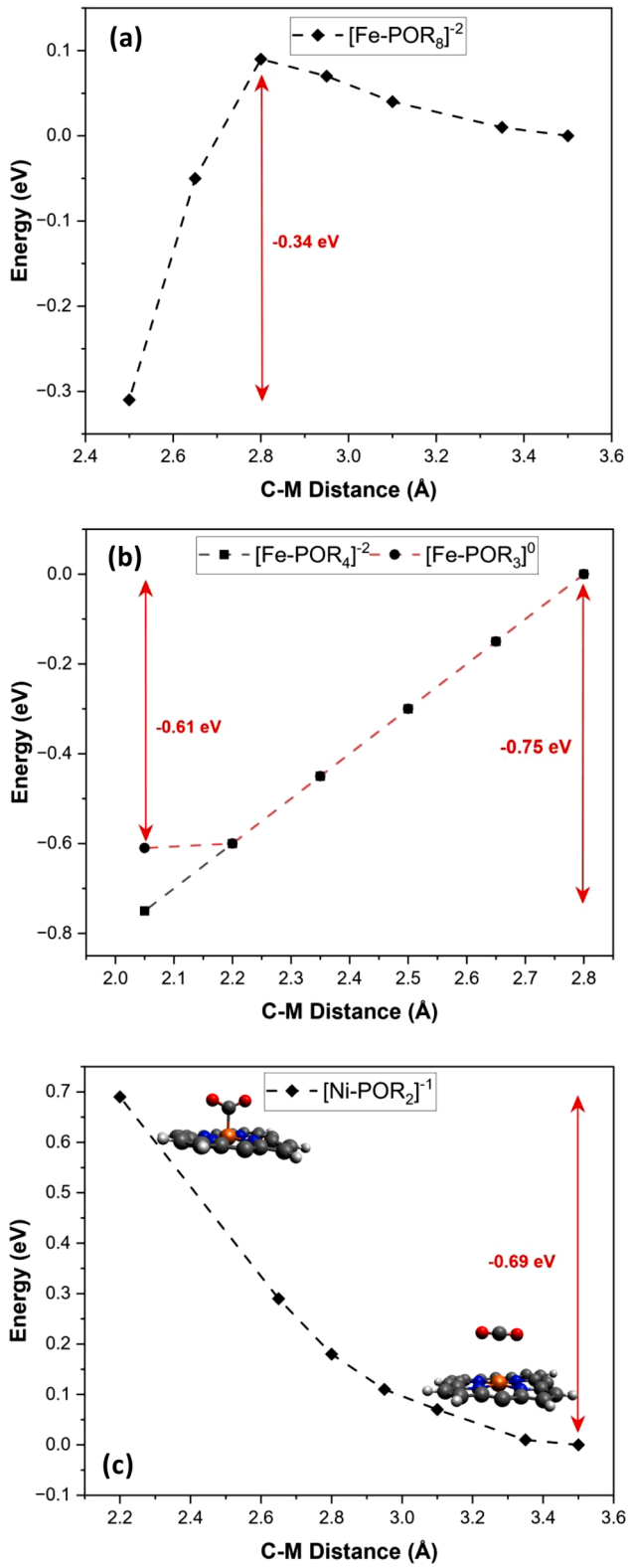


**Fig. 4.** Energy variation (in electronvolts, eV) as a function of the distance between the carbon of $CO_2$ and the metal center of M-POR. The graph investigates the transition from chemisorbed to physisorbed states of $CO_2$ on different metal-POR complexes: (a) $[Fe\text{-}POR_8]^{2-}$; (b) $[Fe\text{-}POR_4]^{2-}$ and $[Fe\text{-}POR_3]^{0}$; (c) $[Ni\text{-}POR_2]^{-1}$. The energy of the physisorbed state serves as the reference point (0 eV), and the red arrows indicate the energy difference between the chemisorbed and physisorbed states. (For interpretation of the references to color in this figure legend, the reader is referred to the web version of this article.)

stable d[10] configuration.

The binding of $CO_2$ to M-POR was further analysed based on the coordination modes presented in Fig. 7, as proposed by Rzepa [55,56]: (1) Bonded interaction with the metal via just one O atom; (2) Bonded interaction via just the central C atom; (3) Bonded interaction via the π-face of one of the C = O double bond; (4) Weaker non-bonded interaction via C; (5) Weaker non-bonded interaction via O. Type **1**–**3** have been classified as chemisorbed states while **4** and **5** as physisorbed states.

As detailed in **Table S3** of Supporting Information, M-PORs with the metal in the electronic configurations d[6], d[7], d[8], and d[9] generally favour chemisorption. Specifically, d[6] and d[7] systems tend to favour bonding of type 1, while d[8] and d[9] systems favour type 2 chemisorption through the central C atom of $CO_2$. Fe-PORs primarily favour type 1 binding, while only seven systems consisting of Ni, Fe, and Co favour type 2 binding. No M-PORs were found to bind to the metal centre of M-POR through the π-face of one of the C=O double bonds. 62 systems physisorbed to M with the electron configuration of the metal varying from d[8], d[9], and d[10] across all metal centres. In comparison, only 20 systems physisorbed through the oxygen atom, with the d[10] configuration being the most common. It is worth noting that the ligands do not appear to influence the type of binding; instead, the metal centre and the overall charge play a more significant role in determining whether chemisorption or physisorption occurs.

To further understand the charge transfer or conjugative interaction in these systems, natural bond order (NBO) analysis was also conducted. **Table S4** shows the M-POR charge donation to $CO_2$ is a result of the M-POR···$CO_2$ complexation. The largest charge transferred to $CO_2$ is by $[Cu\text{-}POR_5]^{-2}$, $[Fe\text{-}POR_1]^{-2}$, and $[Fe\text{-}POR_4]^{-2}$. For $[Cu\text{-}POR_5\cdots CO_2]^{-2}$, this also accompanied by a drastic shift of the C—O stretching mode of adsorbed $CO_2$ to lower frequencies (1874 $cm^{-1}$) compared to the value in the isolated gas phase molecule (2285 $cm^{-1}$) suggesting weakening of the C—O bond in this complex. Systems $[Fe\text{-}POR_1]^{-2}$ and $[Fe\text{-}POR_4]^{-2}$ have the same 3d orbital occupancy of 7.10 and 7.11, respectively (see **Table S5**) but very different orbital splitting of 33.8 kcal $mol^{-1}$ and 95.1 kcal $mol^{-1}$. The extra $–CH_3$ groups in $[Fe\text{-}POR_4]^{-2}$ may lead to stronger interactions between the porphyrin and the $CO_2$ leading to increased splitting, making it more difficult to activate $CO_2$. The systems $[Fe\text{-}POR_1]^{0}$ and $[Fe\text{-}POR_3]^{0}$ have the same metal centre and overall charge but differ in ligands. In $Fe\text{-}POR_3$, the sulfonic acid group on each benzene ring makes the ligands electron-withdrawing, as evidenced by the orbital splitting being significantly higher (−137 kcal $mol^{-1}$) than in $Fe\text{-}POR_1$ (−53.7 kcal $mol^{-1}$).

Donor acceptor interactions was also considered by applying the second order perturbation theory analysis [57]. We have found that in system $[Ni\text{-}POR_1]^{-1}$, where electron donating phenyl groups [58] are in the ligands, there is significant energy gained (131 kcal $mol^{-1}$) by the transfer of electron density from the Ni to the C. There is also some significant backdonation (21.7 kcal $mol^{-1}$) from a sigma from the $CO_2$. However, in $[Ni\text{-}POR_3]^{-1}$, there are electron-withdrawing carboxylic acid groups. The energy required for electron density to be donated from Ni to C of $CO_2$ is similar to that required for backdonation (6.80 kcal $mol^{-1}$ and 6.40 kcal $mol^{-1}$, respectively), highlighting the importance of having electron donating groups in the ligand structure. This is further supported by $[Ni\text{-}POR_1]^{-1}$, which shows more donation than $[Ni\text{-}POR_3]^{-1}$ (**Table S4**). Furthermore, $[Ni\text{-}POR_3]^{-1}$ also has a smaller 3d orbital occupancy (3.79) than $[Ni\text{-}POR_1]^{-1}$ (3.98), but since these systems have the same charge, this suggests some electron transfer to ligands and $CO_2$ in the $[Ni\text{-}POR_3]^{-1}$ complex.

## 4. Conclusions

A computational investigation of the interaction between $CO_2$ and metalloporphyrin catalysts for electrochemical $CO_2$ reduction was carried out using comprehensive density functional theory calculations. Atomistic models of 110 M-PORs were generated by varying the metal

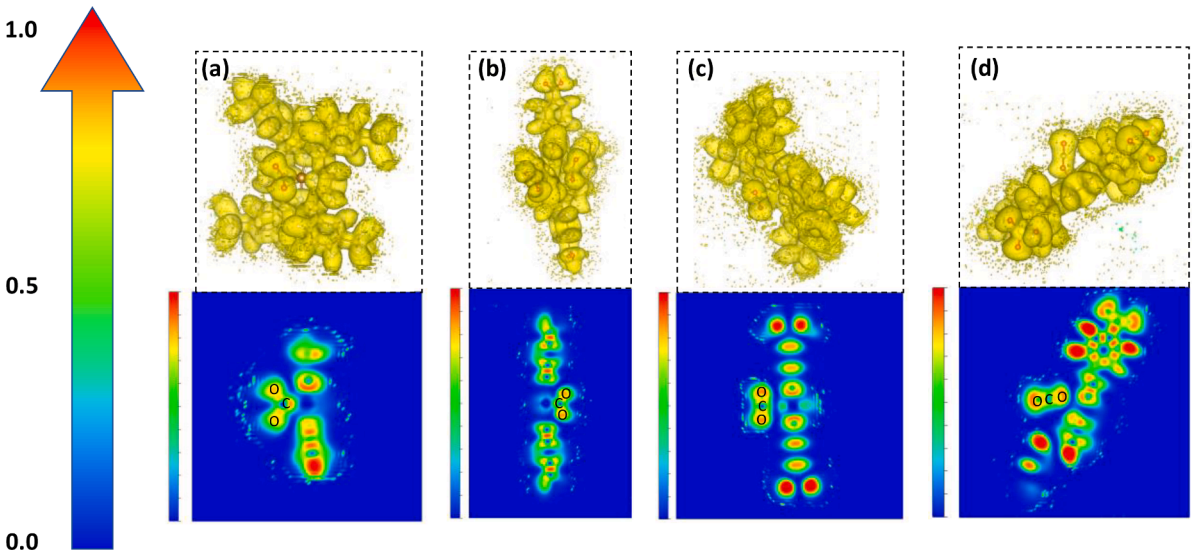


**Fig. 5.** Electron localization maps and corresponding side profile of $CO_2$ coordinated to the following M-PORs: **(a)** $[Ni\text{-}POR_2]^{-1}$; **(b)** $[Fe\text{-}POR_4]^{-2}$; **(c)** $[Fe\text{-}POR_3]^{0}$; **(d)** $[Fe\text{-}POR_8]^{-2}$. The blue and red areas correspond to low and high electron localization, respectively. (For interpretation of the references to color in this figure legend, the reader is referred to the web version of this article.)

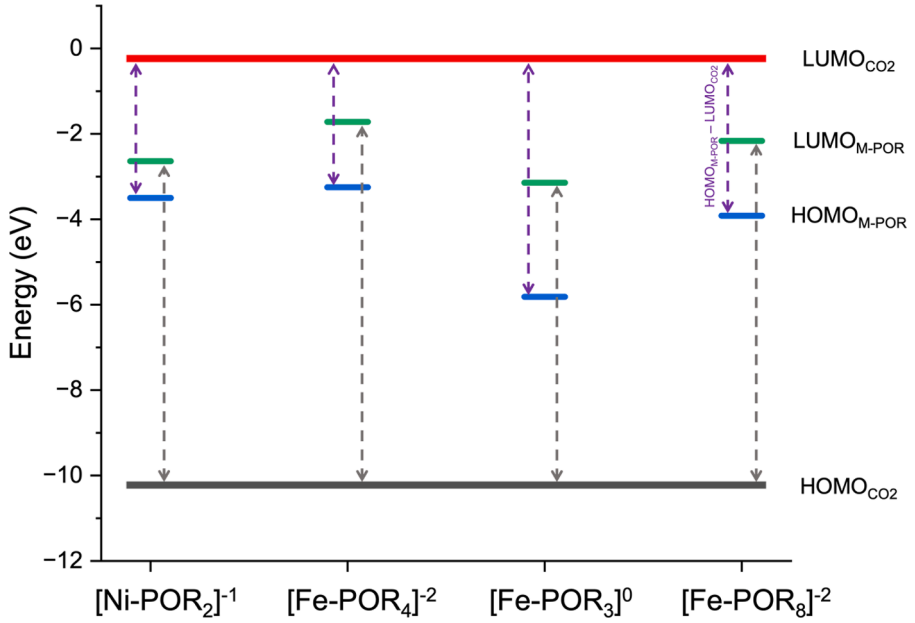


**Fig. 6.** Energy diagram of the HOMO and LUMO orbitals of both the pristine $CO_2$ and the bare M-POR where the grey line is the HOMO for $CO_2$, and the red line is the LUMO for $CO_2$. The green points are the LUMO for M-POR and the blue for the HOMO of M-POR. (For interpretation of the references to color in this figure legend, the reader is referred to the web version of this article.)

centre, oxidation state, and peripheral ligands to understand how these factors affect $CO_2$ adsorption and activation, the first step in electrocatalytic $CO_2$ reduction reaction. When looking at HOMO-LUMO energies, we have found that the charge migration from the M-POR to the $CO_2$ molecule is more favourable when this is accompanied by $CO_2$ bending. Based on defined criteria for characterizing the activation of $CO_2$ (binding energy, C–O bond elongation, O–C–O bending, charge transfer), 16 systems were shortlisted. Both Ni-POR catalysts have a d[9] electronic configuration for Ni, while $[Fe\text{-}POR_2]^{0}$, $[Fe\text{-}POR_3]^{0}$, and $[Fe\text{-}POR_4]^{0}$ among neutral iron-based catalysts exhibit the highest $CO_2$ activation effectiveness. $[Fe\text{-}POR]^{-2}$ and $[Co\text{-}POR_{2,4,5}]^{-1}$ have a d[8] configuration, moderately effective for $CO_2$ activation, with $[Co\text{-}POR_{2,4,5}]^{-1}$ being the least reactive. [Cu-POR] catalysts, with a stable d[10] configuration, show poor $CO_2$ activation. The use of only physisorption and chemisorption was found to be insufficient to fully represent the complexity of $CO_2$ interactions with M-POR. To better understand these interactions, $CO_2$ binding was classified into four categories (F-P, F-C, C-1, and C-2) and in terms of the type of coordination, by either the oxygen or carbon atom of the $CO_2$ molecule. Natural bond order analysis revealed the impact of electron withdrawing groups in the system in increasing orbital splitting, leading to more difficult $CO_2$ activation. Moreover, second order perturbation theory analysis confirms that the presence of electron-donating groups in the ligand structure enhances the activation of the $CO_2$ molecule.

## CRediT authorship contribution statement

**Amira Tasnima Uddin:** Writing – original draft, Methodology,

**Table 3**
Table showing all systems considered in this study against the criteria used to determine if the M-POR activates $CO_2$. The '✓' denotes that the system meets the criteria, a '?' means it is close to meeting the criteria, blank means it has not met the criteria, and 'Y' means the system is activating $CO_2$.

| | 1 | 2 | 3 | 4 | Activated? | | 1 | 2 | 3 | 4 | Activated? | | 1 | 2 | 3 | 4 | Activated? |
|---|---|---|---|---|---|---|---|---|---|---|---|---|---|---|---|---|---|
| $[Ni1]^0$ | ✓ | | | | | $[Fe3]^{-2}$ | ? | | | | | $[Cu7]^0$ | ? | | | | |
| $[Ni1]^{-1}$ | | ✓ | ✓ | ✓ | Y | $[Fe4]^0$ | ? | ✓ | ✓ | ? | Y | $[Cu7]^{-1}$ | ? | | | | |
| $[Ni1]^{-2}$ | ? | | | | | $[Fe4]^{-1}$ | | | | | | $[Cu7]^{-2}$ | ? | | | | |
| $[Ni2]^0$ | ? | | | | | $[Fe4]^{-2}$ | ? | ? | ✓ | ✓ | Y | $[Cu8]^0$ | ? | | | | |
| $[Ni2]^{-1}$ | | | ? | ✓ | | $[Fe5]^0$ | ? | ✓ | ✓ | ? | Y | $[Cu8]^{-1}$ | ? | | | | |
| $[Ni2]^{-2}$ | ? | | | | | $[Fe5]^{-1}$ | ? | | | | | $[Cu8]^{-2}$ | ? | | | | |
| $[Ni3]^0$ | ? | | | | | $[Fe5]^{-2}$ | ? | | | | | $[Cu9]^0$ | ? | | | | |
| $[Ni3]^{-1}$ | ? | | ✓ | ✓ | Y | $[Fe6]^0$ | ? | | ✓ | ? | | $[Cu9]^{-1}$ | ? | | | | |
| $[Ni3]^{-2}$ | ? | | | | | $[Fe6]^{-1}$ | ? | | | | | $[Cu9]^{-2}$ | ? | | | | |
| $[Ni4]^0$ | | | | | | $[Fe6]^{-2}$ | ? | | | | | $[Co1]^0$ | ? | | | | |
| $[Ni4]^{-1}$ | | | | | | $[Fe7]^0$ | ? | | ✓ | ? | | $[Co1]^{-1}$ | ? | | | | |
| $[Ni4]^{-2}$ | ? | | | | | $[Fe7]^{-1}$ | ? | | | | | $[Co1]^{-2}$ | ? | | | | |
| $[Ni5]^0$ | | | | | | $[Fe7]^{-2}$ | ? | | | | | $[Co2]^0$ | | | | | |
| $[Ni5]^{-1}$ | | | | | | $[Fe8]^0$ | ? | ✓ | ✓ | ? | Y | $[Co2]^{-1}$ | ? | | ✓ | ✓ | Y |
| $[Ni5]^{-2}$ | ? | | | | | $[Fe8]^{-1}$ | ? | | | | | $[Co2]^{-2}$ | ? | | | | |
| $[Ni6]^0$ | | | | | | $[Fe8]^{-2}$ | ? | | | | | $[Co3]^0$ | ? | | | | |
| $[Ni6]^{-1}$ | ? | | | | | $[Fe9]^0$ | ? | | | | | $[Co3]^{-1}$ | ? | | | | |
| $[Ni6]^{-2}$ | ? | | | | | $[Fe9]^{-1}$ | | | | | | $[Co3]^{-2}$ | ? | | | | |
| $[Ni7]^0$ | ? | | | | | $[Fe9]^{-2}$ | ? | | ✓ | | | $[Co4]^0$ | ✓ | | | | |
| $[Ni7]^{-1}$ | | | | | | $[Cu1]^0$ | ? | | | | | $[Co4]^{-1}$ | ? | | ✓ | ✓ | Y |
| $[Ni7]^{-2}$ | ? | | | | | $[Cu1]^{-1}$ | ? | | | | | $[Co4]^{-2}$ | ? | | | | |
| $[Ni8]^0$ | ? | | | ✓ | | $[Cu1]^{-2}$ | ? | | | | | $[Co5]^0$ | ? | | | | |
| $[Ni8]^{-1}$ | ? | | | | | $[Cu2]^0$ | ? | | | | | $[Co5]^{-1}$ | ? | ? | ✓ | ✓ | Y |
| $[Ni8]^{-2}$ | ? | | | | | $[Cu2]^{-1}$ | ? | | | | | $[Co5]^{-2}$ | ? | | | | |
| $[Ni9]^0$ | ? | | | | | $[Cu2]^{-2}$ | ? | | | | | $[Co6]^0$ | ? | | | | |
| $[Ni9]^{-1}$ | | | | | | $[Cu3]^0$ | ? | | | | | $[Co6]^{-1}$ | ? | | | | |
| $[Ni9]^{-2}$ | ? | | | | | $[Cu3]^{-1}$ | ? | | | | | $[Co6]^{-2}$ | ? | | | | |
| $[Ni11]^{-2}$ | ? | | | | | $[Cu3]^{-2}$ | ? | | | | | $[Co7]^0$ | | | | | |
| $[Ni10]^{-2}$ | ? | | | | | $[Cu4]^0$ | ? | | | | | $[Co7]^{-1}$ | ? | | | | |
| $[Fe1]^0$ | ? | ✓ | ✓ | ? | Y | $[Cu4]^{-1}$ | ? | | | | | $[Co7]^{-2}$ | ? | | | | |
| $[Fe1]^{-1}$ | ? | | | | | $[Cu4]^{-2}$ | | | | | | $[Co8]^0$ | ? | | | | |
| $[Fe1]^{-2}$ | ? | ? | ✓ | ✓ | Y | $[Cu5]^0$ | | | | | | $[Co8]^{-1}$ | ? | | | | |
| $[Fe2]^0$ | ? | ✓ | ✓ | ? | Y | $[Cu5]^{-1}$ | ? | | | | | $[Co8]^{-2}$ | ? | | | | |
| $[Fe2]^{-1}$ | ? | | | | | $[Cu5]^{-2}$ | ? | | ✓ | ✓ | Y | $[Co9]^0$ | | | | | |
| $[Fe2]^{-2}$ | ? | | | | | $[Cu6]^0$ | ? | | | | | $[Co9]^{-1}$ | ? | | | | |
| $[Fe3]^0$ | ? | ✓ | ✓ | ? | Y | $[Cu6]^{-1}$ | ? | | | | | $[Co9]^{-2}$ | ? | | | | |
| $[Fe3]^{-1}$ | | | | | | $[Cu6]^{-2}$ | ? | | | | | | | | | | |

| | 1 | 2 | 3 | 4 | 5 |
|---|---|---|---|---|---|
| | 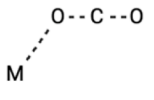 | 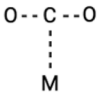 | 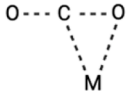 | 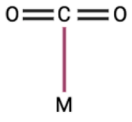 | 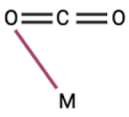 |
| Number of systems | 20 | 7 | 0 | 62 | 21 |

**Fig. 7.** $CO_2$ binding on the metal centre of M-POR: (1) bonded interaction with M via just one O; (**2**) bonded interaction via the C; (**3**) bonded interaction via the π-face of one C=O double bond; (**4**) weaker non-bonded interaction via C and (**5**) O.

Investigation, Formal analysis, Data curation, Conceptualization. **Qi Zhao:** Writing – review & editing, Methodology, Formal analysis. **Dimitrios Toroz:** Writing – review & editing, Formal analysis. **Rachel Crespo-Otero:** Writing – review & editing, Supervision, Methodology, Funding acquisition, Conceptualization. **Devis Di Tommaso:** Writing – review & editing, Supervision, Methodology, Funding acquisition, Conceptualization.

## Declaration of competing interest

The authors declare that they have no known competing financial interests or personal relationships that could have appeared to influence the work reported in this paper.

## Data availability

Data will be made available on request.

## Acknowledgements

Q.Z. thanks the China Scholarship Council for financial support. This work was supported by UK's Royal Society International Exchanges Cost Share (IEC\R3\193106). We thank Prof. Hirotomo Nishihara and his team at Tohoku University for useful discussions. We are grateful to the UK Materials and Molecular Modelling Hub for computational resources, which is partially funded by EPSRC (EP/P020194/1). This research utilized Queen Mary's Apocrita HPC facility, supported by QMUL Research-IT. https://doi.org/10.5281/zenodo.438045.

## Supplementary materials

Supplementary material associated with this article can be found, in the online version, at doi:10.1016/j.mcat.2024.114386.

## References


[1] W. Zhang, Y. Hu, L. Ma, G. Zhu, Y. Wang, X. Xue, R. Chen, S. Yang, Z. Jin, Progress and perspective of electrocatalytic $CO_2$ reduction for renewable carbonaceous fuels and chemicals, Adv. Sci. 5 (2018) 205–239.

[2] J.D. Shakun, P.U. Clark, F. He, S.A. Marcott, A.C. Mix, Z. Liu, B. Otto-Bliesner, A. Schmittner, E. Bard, Global warming preceded by increasing carbon dioxide concentrations during the last deglaciation, Nature 484 (2012) 49–54.

[3] V.K. Arora, J.F. Scinocca, G.J. Boer, J.R. Christian, K.L. Denman, G.M. Flato, V. V. Kharin, W.G. Lee, W.J. Merryfield, Carbon emission limits required to satisfy future representative concentration pathways of greenhouse gases, Geophys. Res. Lett. 38 (2011) L05805.

[4] B.M. Tackett, E. Gomez, J.G. Chen, Net reduction of CO2 via its thermocatalytic and electrocatalytic transformation reactions in standard and hybrid processes, Nat. Catal. 2 (2019) 381–386.

[5] J. Zhang, Z. Li, Z. Zhang, K. Feng, B. Yan, Can thermocatalytic transformations of captured CO2 reduce CO2 emissions? Appl. Energy 281 (2021) 116076.

[6] G. Centi, E.A. Quadrelli, S. Perathoner, Catalysis for CO2 conversion: a key technology for rapid introduction of renewable energy in the value chain of chemical industries, Energy Environ. Sci. 6 (2013) 1711.

[7] E.V. Kondratenko, G. Mul, J. Baltrusaitis, G.O. Larrazábal, J. Pérez-Ramírez, Status and perspectives of CO2 conversion into fuels and chemicals by catalytic, photocatalytic and electrocatalytic processes, Energy Environ. Sci. 6 (2013) 3112.

[8] W. Wang, S. Wang, X. Ma, J. Gong, Recent advances in catalytic hydrogenation of carbon dioxide, Chem. Soc. Rev. 40 (2011) 3703.

[9] K. Qi, Y. Zhang, N. Onofrio, E. Petit, X. Cui, J. Ma, J. Fan, H. Wu, W. Wang, J. Li, J. Liu, Y. Zhang, Y. Wang, G. Jia, J. Wu, L. Lajaunie, C. Salameh, D. Voiry, Unlocking direct CO2 electrolysis to C3 products via electrolyte supersaturation, Nat. Catal. 6 (2023) 319–331.

[10] Y.Y. Birdja, E. Pérez-Gallent, M.C. Figueiredo, A.J. Göttle, F. Calle-Vallejo, M.T. M. Koper, Advances and challenges in understanding the electrocatalytic conversion of carbon dioxide to fuels, Nat. Energy 4 (2019) 732–745.

[11] S. Nitopi, E. Bertheussen, S.B. Scott, X. Liu, A.K. Engstfeld, S. Horch, B. Seger, I.E. L. Stephens, K. Chan, C. Hahn, J.K. Nørskov, T.F. Jaramillo, I. Chorkendorff, Chem. Rev. 119 (2019) 7610–7672.

[12] A.M. Appel, J.E. Bercaw, A.B. Bocarsly, H. Dobbek, D.L. Dubois, M. Dupuis, J. G. Ferry, E. Fujita, R. Hille, P.J.A. Kenis, C.A. Kerfeld, R.H. Morris, C.H.F. Peden, A. R. Portis, S.W. Ragsdale, T.B. Rauchfuss, J.N.H. Reek, L.C. Seefeldt, R.K. Thauer, G. L. Waldrop, Chem. Rev. 113 (2013) 6621–6658.

[13] V.P. Indrakanti, J.D. Kubicki, H.H. Schobert, Photoinduced activation of CO2 on Ti-based heterogeneous catalysts: current state, chemical physics-based insights and outlook, Energy Environ. Sci. 2 (2009) 745–758.

[14] Z. Sun, T. Ma, H. Tao, Q. Fan, B. Han, Fundamentals and challenges of electrochemical CO2 reduction using two-dimensional materials, Chemistry. (Easton) 3 (2017) 560–587.

[15] Y. Hori, H. Wakebe, T. Tsukamoto, O. Koga, Electrocatalytic process of CO selectivity in electrochemical reduction of CO2 at metal electrodes in aqueous media, Electrochim. Acta 39 (1994) 1833–1839.

[16] R. Kortlever, I. Peters, S. Koper, M.T.M. Koper, Electrochemical CO2 reduction to formic acid at low overpotential and with high faradaic efficiency on carbon-supported bimetallic Pd–Pt nanoparticles, ACS Catal. 5 (2015) 3916–3923.

[17] E.E. Benson, C.P. Kubiak, A.J. Sathrum, J.M. Smieja, Electrocatalytic and homogeneous approaches to conversion of CO2 to liquid fuels, Chem. Soc. Rev. 38 (2009) 89–99.

[18] B. Innocent, D. Pasquier, F. Ropital, F. Hahn, J.M. Léger, K.B. Kokoh, FTIR spectroscopy study of the reduction of carbon dioxide on lead electrode in aqueous medium, Appl. Catal. B 94 (2010) 219–224.

[19] N. Thonemann, A. Schulte, From laboratory to industrial scale: a prospective LCA for electrochemical reduction of $CO_2$ to formic acid, Environ. Sci. Technol. 53 (2019) 12320–12329.

[20] P. Gotico, Z. Halime, A. Aukauloo, Recent advances in metalloporphyrin-based catalyst design towards carbon dioxide reduction: from bio-inspired second coordination sphere modifications to hierarchical architectures, Dalton Trans. 49 (2020) 2381–2396.

[21] S. Gu, A.N. Marianov, T. Lu, J. Zhong, A review of the development of porphyrin-based catalysts for electrochemical CO2 reduction, Chem. Eng. J. 470 (2023) 144249.

[22] H. Lv, X. Zhang, K. Guo, J. Han, H. Guo, H. Lei, X. Li, W. Zhang, U. Apfel, R. Cao, Coordination tuning of metal porphyrins for improved oxygen evolution reaction, Angew. Chem. Int. Ed. 62 (2023) 1–6.

[23] P. Sen, B. Mondal, D. Saha, A. Rana, A. Dey, Role of 2nd sphere H-bonding residues in tuning the kinetics of $CO_2$ reduction to CO by iron porphyrin complexes, Dalton Trans. 48 (2019) 5965–5977.

[24] B. Mondal, P. Sen, A. Rana, D. Saha, P. Das, A. Dey, Reduction of CO2 to CO by an iron porphyrin catalyst in the presence of oxygen, ACS Catal. 9 (2019) 3895–3899.

[25] C. Costentin, S. Drouet, M. Robert, J.-M. Savéant, A local proton source enhances CO2 electroreduction to CO by a molecular Fe Catalyst, Science 338 (2012) 90–94.

[26] M. Abdinejad, L.F.B. Wilm, F. Dielmann, H.B. Kraatz, Electroreduction of $CO_2$ catalyzed by nickel imidazolin-2-ylidenamino-porphyrins in both heterogeneous and homogeneous molecular systems, ACS Sustain. Chem. Eng. 9 (2021) 521–530.

[27] Z. Cao, S.B. Zacate, X. Sun, J. Liu, E.M. Hale, W.P. Carson, S.B. Tyndall, J. Xu, X. Liu, X. Liu, C. Song, J. Luo, M. Cheng, X. Wen, W. Liu, Tuning gold nanoparticles with chelating ligands for highly efficient electrocatalytic $CO_2$ reduction, Angew. Chem. 130 (2018) 12857–12861.

[28] G. Dutta, A.K. Jana, D.K. Singh, M. Eswaramoorthy, S. Natarajan, Encapsulation of silver nanoparticles in an amine-functionalized porphyrin metal–organic framework and its use as a heterogeneous catalyst for CO2 fixation under atmospheric pressure, Chem. Asian J. 13 (2018) 2677–2684.

[29] X. Zhang, X. Li, D. Zhang, N.Q. Su, W. Yang, H.O. Everitt, J. Liu, Product selectivity in plasmonic photocatalysis for carbon dioxide hydrogenation, Nat. Commun. 8 (2017) 14542.

[30] S. Park, D. Bézier, M. Brookhart, An efficient iridium catalyst for reduction of carbon dioxide to methane with trialkylsilanes, J. Am. Chem. Soc. 134 (2012) 11404–11407.

[31] A. Klinkova, P. De Luna, C.-T. Dinh, O. Voznyy, E.M. Larin, E. Kumacheva, E. H. Sargent, Rational design of efficient palladium catalysts for electroreduction of carbon dioxide to formate, ACS Catal. 6 (2016) 8115–8120.

[32] C. Römelt, S. Ye, E. Bill, T. Weyhermüller, M. van Gastel, F. Neese, Electronic structure and spin multiplicity of iron tetraphenylporphyrins in their reduced states as determined by a combination of resonance raman spectroscopy and quantum chemistry, Inorg. Chem. 57 (2018) 2141–2148.

[33] Z. Masood, Q. Ge, Mechanism and selectivity of electrochemical reduction of CO2 on metalloporphyrin catalysts from DFT studies, Molecules 28 (2023) 1–12.

[34] D. Di Tommaso, H. Cove, D. Toroz, N. Dzade, S.Ruiz Hernandez, D. Santos-Carballal, The effect of the oxidation state of the metal center in metalloporphyrins on the electrocatalytic CO2-to-CO conversion: a density functional theory study, Mol. Catal. 498 (2020) 1–8.

[35] N. Corbin, J. Zeng, K. Williams, K. Manthiram, Heterogeneous molecular catalysts for electrocatalytic CO2 reduction, Nano Res. 12 (2019) 2093–2125.

[36] E. Boutin, L. Merakeb, B. Ma, B. Boudy, M. Wang, J. Bonin, E. Anxolabéhère-Mallart, M. Robert, Molecular catalysis of CO2reduction: recent advances and perspectives in electrochemical and light-driven processes with selected Fe, Ni and Co aza macrocyclic and polypyridine complexes, Chem. Soc. Rev. 49 (2020) 5772–5809.

[37] D. Di Tommaso, D. Di, T.Q. Zhao, R. Crespo-Otero, B.Y. Xia, The role of copper in enhancing the performance of heteronuclear diatomic catalysts for the electrochemical CO2 conversion to C1 chemicals, J. Energy Chem. 85 (2023) 490–500.

[38] H. Shin, K.U. Hansen, F. Jiao, Techno-economic assessment of low-temperature carbon dioxide electrolysis, Nat. Sustain. 4 (2021) 911–919.

[39] J. Ko, B.-K. Kim, J.W. Han, Density functional theory study for catalytic activation and dissociation of CO2 on bimetallic alloy surfaces, J. Phys. Chem. C 120 (2016) 3438–3447.

[40] N. Austin, J. Ye, G. Mpourmpakis, CO2 activation on Cu-based Zr-decorated nanoparticles, Catal. Sci. Technol. 7 (2017) 2245–2251.

[41] E. Aprà, E.J. Bylaska, W.A. de Jong, N. Govind, K. Kowalski, T.P. Straatsma, M. Valiev, H.J.J. van Dam, Y. Alexeev, J. Anchell, V. Anisimov, F.W. Aquino, R. Atta-Fynn, J. Autschbach, N.P. Bauman, J.C. Becca, D.E. Bernholdt, K. Bhaskaran-Nair, S. Bogatko, P. Borowski, J. Boschen, J. Brabec, A. Bruner, E. Cauët, Y. Chen, G.N. Chuev, C.J. Cramer, J. Daily, M.J.O. Deegan, T.H. Dunning, M. Dupuis, K.G. Dyall, G.I. Fann, S.A. Fischer, A. Fonari, H. Früchtl, L. Gagliardi, J. Garza, N. Gawande, S. Ghosh, K. Glaesemann, A.W. Götz, J. Hammond, V. Helms, E.D. Hermes, K. Hirao, S. Hirata, M. Jacquelin, L. Jensen, B.G. Johnson, H. Jónsson, R.A. Kendall, M. Klemm, R. Kobayashi, V. Konkov, S. Krishnamoorthy, M. Krishnan, Z. Lin, R.D. Lins, R.J. Littlefield, A.J. Logsdail, K. Lopata, W. Ma, A. v. Marenich, J. Martin del Campo, D. Mejia-Rodriguez, J.E. Moore, J.M. Mullin, T. Nakajima, D.R. Nascimento, J.A. Nichols, P.J. Nichols, J. Nieplocha, A. Otero-de-la-Roza, B. Palmer, A. Panyala, T. Pirojsirikul, B. Peng, R. Peverati, J. Pittner, L. Pollack, R.M. Richard, P. Sadayappan, G.C. Schatz, W.A. Shelton, D. W. Silverstein, D.M.A. Smith, T.A. Soares, D. Song, M. Swart, H.L. Taylor, G. S. Thomas, V. Tipparaju, D.G. Truhlar, K. Tsemekhman, T. van Voorhis, Á. Vázquez-Mayagoitia, P. Verma, O. Villa, A. Vishnu, K.D. Vogiatzis, D. Wang, J. H. Weare, M.J. Williamson, T.L. Windus, K. Woliński, A.T. Wong, Q. Wu, C. Yang, Q. Yu, M. Zacharias, Z. Zhang, Y. Zhao, R.J. Harrison, NWChem: past, present, and future, J. Chem. Phys. 152 (2020) 184102.

[42] Gaussian 09, Revision E.01, M.J. Frisch, G.W.D.J. Trucks, H.B. Schlegel, G.E. Scuseria, M.A. Robb, J.R. Cheeseman, G. Scalmani, V. Barone, B. Mennucci, G.A. Petersson, H. Nakatsuji, M. Caricato, X. Li, H.P. Hratchian, A.F. Izmaylov, J. Bloino, G. Zheng, Sonnenberg J.L. and Inc Wallingford CT, 2009.

[43] A. Klamt, G. Schürmann, COSMO: a new approach to dielectric screening in solvents with explicit expressions for the screening energy and its gradient, J. Chem. Soc. Perkin Trans. 2 (1993) 799–805.

[44] A. Klamt, The COSMO and COSMO-RS solvation models, WIREs Comput. Mol. Sci. 1 (2011) 699–709.

[45] D. Vega, D. Almeida, AIM-UC: an application for QTAIM analysis, J. Comput. Methods Sci. Eng. 14 (2014) 131–136.

[46] J. Park, M. Cho, Y.M. Rhee, Y. Jung, Theoretical study on the degree of CO2 activation in CO2-coordinated Ni(0) complexes, ACS. Omega 6 (2021) 7646–7654.

[47] N. Austin, B. Butina, G. Mpourmpakis, CO2 activation on bimetallic CuNi nanoparticles, Progr. Natural Sci. 26 (2016) 487–492.

[48] H.-J. Freund, M.W. Roberts, Surface chemistry of carbon dioxide, Surf. Sci. Rep. 25 (1996) 225–273.

[49] S.-G. Wang, X.-Y. Liao, D.-B. Cao, C.-F. Huo, Y.-W. Li, J. Wang, H. Jiao, Factors controlling the interaction of CO2 with transition metal surfaces, J. Phys. Chem. C 111 (2007) 16934–16940.
[50] J. Qiao, Y. Liu, F. Hong, J. Zhang, A review of catalysts for the electroreduction of carbon dioxide to produce low-carbon fuels, Chem. Soc. Rev. 43 (2014) 631–675.
[51] E. Fujita, J. Haff, lb Ralf Sanzenbacher and H. Eliaslc, *High Electrocatalytic Activity of RJ?SS-[NinHTIM](ClC>4)2 and [NinDMC](ClC>4)2 for Carbon Dioxide Reduction (HTIM = 2,3,9,10-Tetramethyl-l,4,8,ll-tetraazacyclotetradecane, DMC = C-mes0-5,12-Dimethyl-l,4,8,ll-tetraazacyclotetradecane)*, 1994, vol. 33.
[52] K. Bujno, R. Bilewicz, L. Siegfried, T. Kaden, Electrochemical behaviour of isomers of a tetraazamacrocyclic Ni(II) complex in solutions saturated with argon, CO and CO2, J. Electroanal. Chem. 407 (1996) 131–140.
[53] B.J. Fisher, R. Eisenberg, Electrocatalytic reduction of carbon dioxide by using macrocycles of nickel and cobalt, J. Am. Chem. Soc. 102 (1980) 7361–7363.
[54] A. Mazheika, Y.-G. Wang, R. Valero, F. Viñes, F. Illas, L.M. Ghiringhelli, S. V. Levchenko, M. Scheffler, Artificial-intelligence-driven discovery of catalyst genes with application to CO2 activation on semiconductor oxides, Nat. Commun. 13 (2022) 419.
[55] S.T. Chacon, M.H. Chisholm, K. Folting, J.C. Huffman, M.J. Hampden-Smith, Allene adducts of ditungsten hexaalkoxides. Three modes of allene coordination to dinuclear centers as seen in the structures of W2(OBu-tert)6(C3H4), W2(OBu-tert)6 (C3H4)2, and W2(OBu-tert)6(C3H4)(CO)2, Organometallics 10 (1991) 3722–3735.
[56] C.H. Lee, D.S. Laitar, P. Mueller, J.P. Sadighi, Generation of a doubly bridging $CO_2$ ligand and deoxygenation of $CO_2$ by an (NHC)Ni(0) complex, J. Am. Chem. Soc. 129 (2007) 13802–13803.
[57] F.M. Fernandez, Introduction to Perturbation Theory in Quantum Mechanics, CRC Press, 2000.
[58] Q. Teng, H.V. Huynh, Determining the electron-donating properties of bidentate ligands by 13C NMR spectroscopy, Inorg. Chem. 53 (2014) 10964–10973.